discrepancy between the calculated and measured cross sections for the isovector transition was not observed. The origin of the differences between these results appears to be in the reaction mechanism. Our measurements show a large-momentum transfer disagreement with the calculations performed with the M3Y effective interaction but not with those performed with the Love and Franey interaction.

1) R. Madey et al., Nucl. Instrum. and Meth. 214, 401 (1983).

2) IUCF Scientific and Technical Report, 1983, p. 35.

3) T.W. Donnelly and G.E. Walker, Ann. of Phys. 60, 209 (1970).

4) J.J. Kelly, Ph.D. Dissertation, M.I.T. (1981). (unpublished).

5) W.G. Love and M.A. Franey, Phys. Rev. C 25, 1073 (1981).

6) G. Bertsch, J. Barysowicz, H. McManus and W.G. Love, Nucl. Phys. A284, 399 (1977).

7) H. Orihara et al., Phys. Rev. Lett. 49, 1318 (1982).

8) K. Hosono et al., Phys. Rev. C 30, 746 (1984).

POLARIZATION-TRANSFER IN $(\vec{p},\vec{n})$ REACTIONS

J.W. Watson, B.D. Anderson, A.R. Baldwin, T. Chittrakarn, B.S. Flanders and R. Madey
Kent State University, Kent, Ohio 44242

P.J. Pella
Hendrix College, Conway, Arkansas 72032

C.C. Foster
Indiana University Cyclotron Facility, Bloomington, Indiana 47405

I. van Heerden
University of the Western Cape, South Afric

One of the most interesting developments in the past half-dozen years in nuclear physics has been the realization that spin-flip modes of excitation become very important at medium energies, especially for isovector excitations. Perhaps the most direct method for studying such excitations is a polarization-transfer measurement. To this end, we began a program of $(\vec{p},\vec{n})$ polarization-transfer measurements about a year ago with a study of the $^{40,48}Ca(\vec{p},\vec{n})^{40,48}Sc$ reactions at 135 MeV.

Cornelius et al.[1] showed that under two simple assumptions (viz. central forces, and a single L-transfer) that spin-flip probabilities, which we will call "S", take on simple, characteristic values. Some of these values are listed in Table 1 for transitions on even-even ($J^{\pi}=0^{+}$) targets. These values for the spin-flip probability "S" are combinations of Clebsch-Gordan coefficients for the angular momentum couplings for the final states. Note that with the exception of the $0^{+} \rightarrow 0^{-}$ transition, all transitions with $\Delta S=1$ have spin-flip probabilities between 1/2 and 3/4. In general, the larger the spin, the closer "S" will be to 3/4. Thus, polarization-transfer measurements are most useful for low values of ΔL where the differences in "S" for different transitions are more pronounced. Polarization-transfer measurements to determine spin-flip probabilities are thus complementary to analyzing-power measurements: polarization-transfer is most useful near 0° where $\Delta L=0$ and $\Delta L=1$ dominate; analyzing powers must vanish identically at 0°.

Table 1: Spin-Flip Probabilities (S)

Transition	ΔS	ΔL	S	Type
$0^+ \rightarrow 0^+$	0	0	0	IAS
$0^+ \rightarrow 1^+$	1	0	2/3	GT
$0^+ \rightarrow 0^-$	1	1	1	"Spin-Flip" Dipole
$0^+ \rightarrow 1^-$	1	1	1/2	
$0^+ \rightarrow 2^-$	1	1	0.7	
$0^+ \rightarrow 1^-$	0	1	0	Non-spin Dipole
$0^+ \rightarrow 2^+$	0	2	0	Collective E2
$0^+ \rightarrow 2^+$	1	2	1/2	Spin-flip E2

What we measure in a $(\vec{p},\vec{n})$ polarization-transfer experiment is p_n, the polarization of the detected neutron. This quantity is related to the polarization of the incoming proton p_p, and to the "transverse polarization transfer coefficient" $K_y^{y'}$ (Madison convention) as follows:

$$(1 + p_p A_y(\Theta))P_n = P(\Theta) + p_p K_y^{y'}(\Theta)$$

where $A_y(\Theta)$ and $P(\Theta)$ are the analyzing power and the polarization function for the reaction, respectively. Since $A_y(\Theta)$ and $P(\Theta)$ vanish identically at 0°, this expression simplifies to:

$$P_n = p_p K_y^{y'}(0°)$$

Thus at 0°, $K_y^{y'}$ is the ratio of the outgoing neutron polarization to the incoming proton polarization.

The spin-flip probability "S" is related to $K_y^{y'}$ as:

$$S = (1 - K_y^{y'})/2.$$

From measurement of p_n, we can determine $K_y^{y'}$ and S.

The experiment was performed with the beam-swinger facility. The flight path from the target to the primary scatterers of the polarimeter was 35m, which provided a satisfactory compromise between energy resolution (about 1 MeV) and counting rate. The energy resolution was limited primarily by the 10 cm thickness of the primary scatterers of the polarimeter.

The neutron polarimeter is shown schematically in Fig. 1. It utilizes the analyzing power of n-p scattering from the hydrogen nuclei in organic scintillators. This analyzing power is typically +0.5 near a laboratory scattering angle of 25° for the energies of interest in these experiments. The primary scatterers are three vertically-mounted mean-timed scintillators 10 cm thick in the direction of the incident neutron flux, 12.5 cm wide and 1.02 m high. Scattered neutrons are detected with two sets (left and right) of vertically-mounted mean-timed "side detectors". Each set consists of three scintillators 10 cm thick, 25.4 cm wide and 1.02 m high. The side detectors are located at a mean flight path of 1 m from the primary scatterers at a mean scattering angle of 22.5°, which is the angle for the maximum in $A_y^2\sigma(\Theta_{n-p})$ for n-p scattering at the relevent neutron energies. The product $A_y^2\sigma$ is the usual figure-of-merit for a polarimeter.

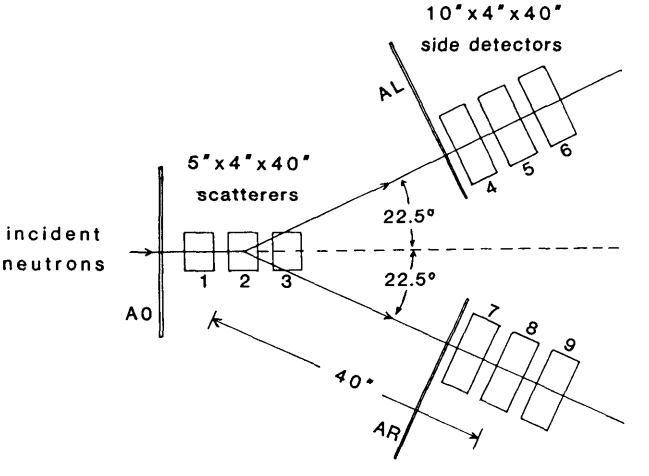

Figure 1. The geometry of the neutron polarimeter, as seen from above.

From the information specifying which detectors were involved in a given event and the positions of interaction in those two scintillators, we can reconstruct (off-line) r, θ, and φ. These co-ordinates and the velocity of the scattered neutron are then compared with free n-p kinematics to eliminate a substantial fraction of (n,np) quasi-free scattering events from the carbon nuclei in the primary scatterers. These quasi-free events are the principal souce of background in the polarimeter. When we optimized the off-line cuts on θ, φ, quasi-free background rejection, and the pulse-height thresholds in the primary and side detectors, we obtained the following performance characteristics for our polarimeter:

$\bar{A}_y$ (average analyzing power) = 0.275 ± 0.010

E (efficiency) = 2.4×10^{-3}

These values were obtained from data for the $^{14}C(p,n)^{14}N$ (2.31 MeV) reaction which is a $0^+ \rightarrow 0^+$ reaction with $K_y^{y'} = 1$, and from the $^{12}C(p,n)^{12}N$ (g.s.) and $^{48}Ca(p,n)^{48}Sc$ (2.52 MeV) reactions where we know the cross sections from previous measurements.

Note that these values for $\bar{A}y$ and E imply a data-taking efficiency that is several times larger than other neutron polarimeters currently in use at medium energies. Because of the intrinsic left/right nature of its design, an especially useful feature of this polarimeter is that it has a useful on-line analyzing power of about 15% with no cuts other than pulse-height thresholds. This fact means that on-line results are readily obtainable without using valuable beam to determine and set up the necessary calibrations for a more complete analysis.

Figure 2 shows our 0° data for the $^{48}Ca(p,n)^{48}Sc$ reaction. Panel (a) is the neutron energy spectrum for all events that passed our final software cuts; the 0+

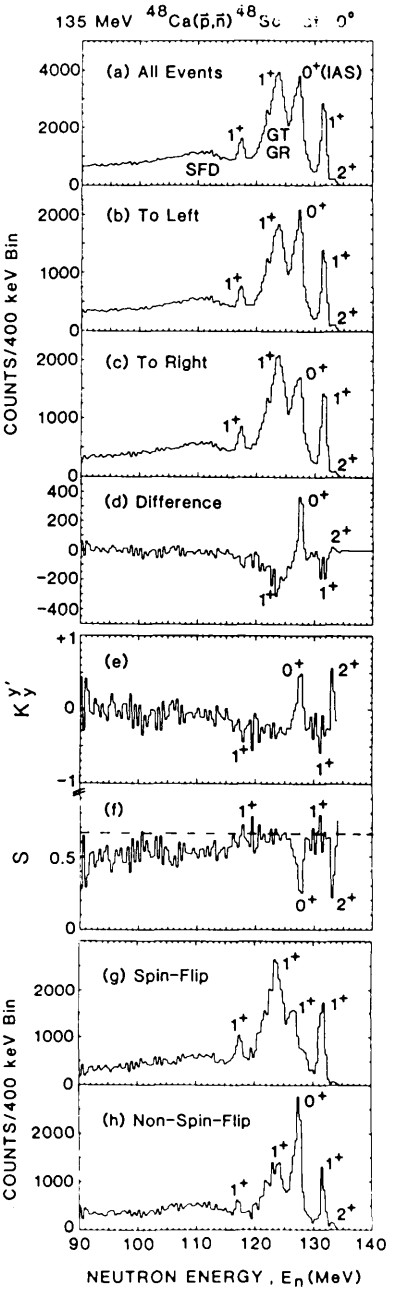

Figure 2. Spectra from the $^{48}Ca(\vec{p},\vec{n})^{48}Sc$ reaction at 135 MeV and 0°: (a) is the spectrum of all neutrons satisfying software cuts; (b) and (c) are spectra of neutrons scattering to the left and to the right in the polarimeter; (d) is the differences of spectra (c) and (b); (e) and (f) are spectra of $K_y^{y'}$ and $S=(1-k_y^{y'})/2$; (g) and (h) are the "spin-flip" and "non-spin'flip" spectra respectively.

isobaric-analog state (IAS), known 1^+ states, including the Gamow-Teller Giant Resonance (GTGR) and the "spin-flip" dipole (SFD) region are labeled. Panels (b) and (c) show the spectra of neutrons that scattered in the polarimeter to the "left" and to the "right", respectively, in the Madison convention. We see immediately a difference between neutrons from the 0^+ IAS and from the 1^+ GTGR; the former scatter preferentially to the left, the latter to the right, indicating different signs to the neutron polarization. This observation shows up even more clearly in panel (d) which shows the "left" minus "right" difference spectrum. Panels (e) and (f) show the spectra of KY'_y and S, defined above. We see that regions of assumed 1+ strength indeed have values of S near 2/3, as indicated by the dashed line. When we multiply the spectrum of all events in panel (a) by S, we generate a "spin-flip spectrum"; multiplying the "all events" spectrum by (1-S) generates a "non-spin-flip spectrum". These results are shown in panels (g) and (h). The 0+ IAS shows up exclusively in the non-spin-flip spectrum, (as required for a $0^+ \rightarrow 0^+$ transition), and the 1^+ states show up with 2/3 of their strength in the spin-flip spectrum, as suggested by Table 1.

Figure 3 shows the spectrum of all events, the spin-flip spectrum and the non-spin-flip spectrum for the $^{40}Ca(p,n)^{40}Sc$ reaction at 0° and 135 MeV. The presumed SFD region (E_n = 105 to 110 MeV; Q = -20 to -25 MeV) dominates the spectrum of all events; the spin-flip and non-spin-flip spectra show marked differences, however, with the SFD strength more sharply concentrated in the non-spin-flip spectrum.

In Fig. 4, we show a comparison of the S spectra for both ^{40}Ca and ^{48}Ca at 0°, but with coarser binning (1 MeV) to reduce statistical fluctuations. For neutron energies between 90 and 105 MeV ("above the SFD region"), we see that there is no appreciable difference between these two targets. This result is especially significant because ^{40}Ca is a spin-saturated self-conjugate target and can have no G-T strength, except for that from ground-state correlations (which presumably produce the two weak 1+ states at low excitation energy); therefore, we can conclude that there is no evidence in the spin-flip spectra that would point unambiguously to residual G-T strength in this part of the continuum. This result does not rule

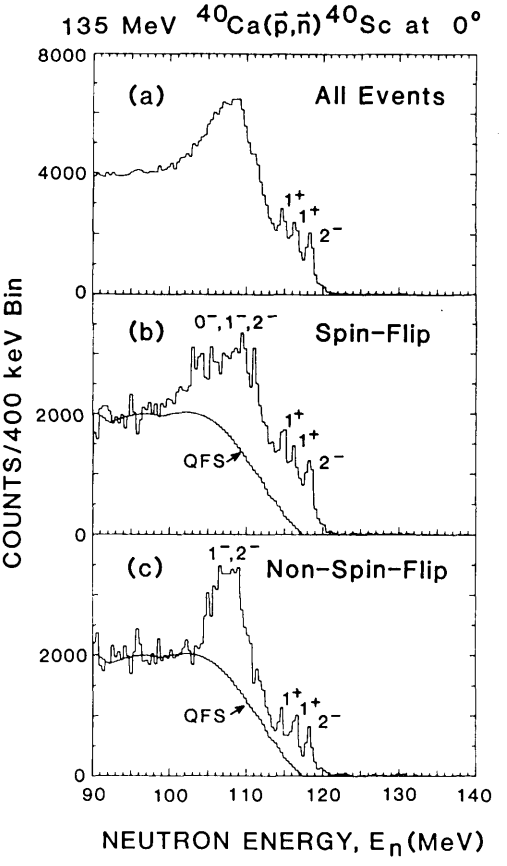

Figure 3. Spectra for the $^{40}Ca(\vec{p},\vec{n})^{40}Sc$ reaction at 135 MeV and 0°: (a) is the spectrum of all neutrons satisfying software cuts; (b) and (c) are "spin-flip" and "non-spin-flip" spectra respectively. The solid lines are plane-wave quasi-free scattering (with Pauli blocking) background calculations, normalized to the data.

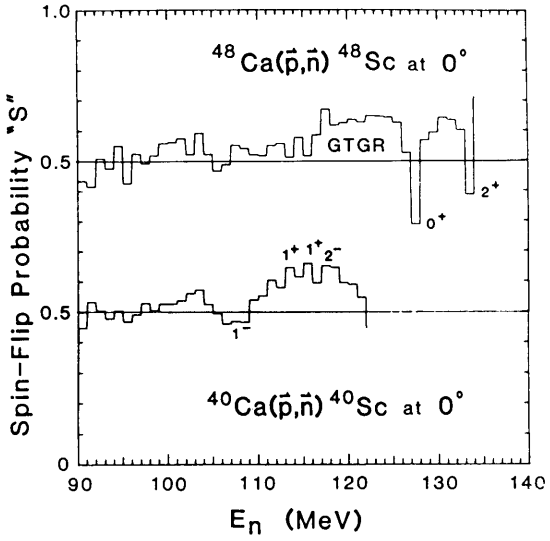

Figure 4. Spectra of the spin-flip probability S ($S=(1-K_y'/2)$) for the 135 MeV (p,n) reactions on ^{40}Ca and ^{48}Ca at 0°.

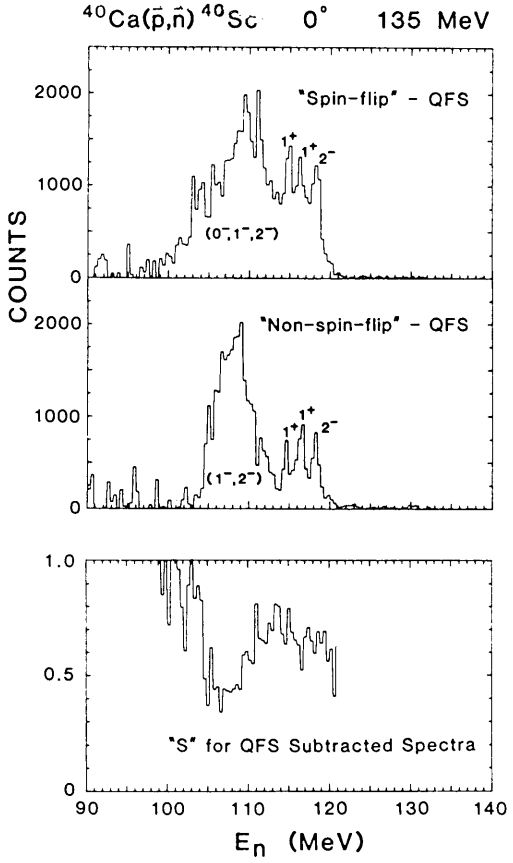

Figure 5. (a) and (b): Spin-flip and non-spin-flip spectra for the 135 MeV $^{40}Ca(p,n)^{40}Sc$ reaction at 0°, after subtraction of the quasi-free scattering backgrounds shown in Fig. 3. (c): The spin-flip probability S derived from spectra (a) and (b) (c=a/(a+b)).

out such strength, but does not provide any support for suggestions that the continuum in this Q-value region contains the missing G-T sum-rule strength.[2] Note, however, that the region labeled "GTGR" for ^{48}Ca in Fig. 4 extends down to about E=115 MeV, which is well below the 16.8 MeV 1+ state; the spin-flip probability (S) in this region is identical to S for the main peak of the GTGR (S=2/3). This is consistent with our earlier analysis of cross-section measurements, which indicate that there is a significant amount of G-T strength (~20% of the sum rule) in the continuum immediately above the GTGR.

Returning to Fig. 3, we show also a plane-wave quasi-free scattering (with Pauli blocking) background normalized to the spectra at E_n=90 to 95 MeV. When we subtract this background, we obtain the spectra in Fig. 5. Since 0^-, 1^- and 2^- states have distinctly different values for S (1, 0.5, 0.7 respectively), this type of decomposition into a spin-flip and a non-spin-flip spectrum can be used to determine approximately the distribution of 0^-, 1^-, and 2^- strength, as indicated in the bottom panel of Fig. 5. Note that values of S smaller than 1/2 indicate the presence of a small amount of non-spin-dipole strength which can only be 1^-, and will be excited relatively weakly at these bombarding energies. The distribution of spin-flip and non-spin-flip strength in Fig. 5 is in good qualitative agreement with distorted-wave impulse approximation predictions based on one-particle-one-hole wave-functions from Donnelly and Walker.[3]

In summary, we measured the transverse polarization-transfer coefficient $K_y^{y'}$ for the 135 MeV $(\vec{p},n)$ reaction on ^{40}Ca and ^{48}Ca. When we compare continuum spin-flip probabilities for these targets in the Q-value region from 30 to 45 MeV, we find no clear evidence for "hidden" G-T strength in this region; however, we do find indications for continuum G-T strength in this region; however, we do find indications for continuum G-T strength in the region between the main peak of the GTGR and the SFD region. Also, we observe clear differences in the distributions of spin-flip and non-spin-flip strength for ^{40}Ca in the Q-value region from 20 to 30 Mev, which we interpret in terms of the well-known Giant-Dipole ($\Delta L=1$, $\Delta S=0$) resonance ($J^{\pi}=1^-$) and the Spin-Flip-Dipole ($\Delta L=1$, $\Delta S=1$) resonance ($J^{\pi}=1^-$, 2^-, 3^-).

1) W.D. Cornelius, J.M. Moss and T. Yamaya, Phys. Rev. C 23, 1364 (1980).

2) G.F. Bertsch and I. Hamamoto, Phys. Rev. C 26, 1323 (1982).

3) T.W. Donnelly and G.E. Walker, Annals of Phys. 60, 209 (1970).